Hutnické listy – *Metallurgical Journal*
Speciální vydání / Special Issue, roč. / vol. LXXIX
ISSN Online: 3029-8350

Integrated CFD Models for Optimizing Scrap Melting in DC EAF

Integrované CFD modely pro optimalizaci tavení šrotu ve stejnosměrné EOP

Shiyu Wang[1], Orlando Ugarte[1], Tyamo Okosun[1], Sunday Abraham[2], Yufeng Wang[2], Randy Petty[2], Chenn Q.Zhou[1]

[1] Center for Innovation through Visualization and Simulation (CIVS) and Steel Manufacturing Simulation and Visualization Consortium (SMSVC), Purdue University Northwest; Hammond, IN, U.S.A. *Correspondence: ougarte@pnw.edu; Tel.: 1-219-989-2089

[2] SSAB Americas, Muscatine, IA, U.S.A.

Abstract

In the U.S., ~70% of steel is produced in electric arc furnaces (EAFs), and significant investment is devoted to increase EAF production capacity. EAFs integrate chemical and electrical energy to melt scrap, precipitating phase changes and reactions that need to be controlled to achieve the desired molten steel. The multi-phenomena nature of EAF operations presents challenges for optimization. This study applies an advanced CFD methodology to simulate the operation of an industrial DC-EAF to study the impact of electrical arc power on melting. Namely, a CFD tool integrating a coherent-jet model, a DC arc heating model and a scrap melting model is applied to a DC-EAF heat provided by SSAB. After validating CFD predictions against actual data, simulations of scenarios with modified arc power (10% and 20% reduction from baseline) are performed. All other conditions such as burner power and charge recipe remain the same. Results indicate that each 10% power reduction extends the melting time for 60 tonnes of scrap by two minutes. Also, a boost in melting performance is observed when the average molten bath temperature rises above the liquidus temperature. Non-uniformity of arc heating is also described and potential optimization of EAF melting is discussed.

Keywords: *electric arc furnace, DC, arc heating, CFD, scrap layering, melting*

Abstrakt

V USA se přibližně 70% oceli vyrábí v elektrických obloukových pecích (EOP) a významné investice směřují do zvyšování jejich výrobní kapacity. Elektrické obloukové pece kombinují chemickou a elektrickou energii k tavení šrotu, přičemž dochází k fázovým přeměnám a reakcím, které je nutné řídit pro dosažení požadovaného stavu roztavené oceli. Více-jevová povaha provozu EOP představuje významnou výzvu z hlediska optimalizace. Tato studie využívá pokročilou metodiku CFD k simulaci provozu průmyslové stejnosměrné elektrické obloukové pece (DC-EAF) za účelem posouzení vlivu výkonu elektrického oblouku na proces tavení. Konkrétně je aplikován CFD nástroj integrující model koherentního proudu, model ohřevu stejnosměrným obloukem a model tavení šrotu na případ průmyslové DC-EAF dodané společností SSAB. Po validaci výsledků CFD simulací na základě reálných provozních dat byly provedeny simulace scénářů se sníženým výkonem oblouku (o 10% a 20% oproti referenčnímu stavu), přičemž ostatní parametry, jako výkon hořáků a složení vsázky, zůstaly nezměněny. Výsledky ukazují, že každé snížení výkonu o 10% prodlužuje dobu tavení 60 tun šrotu přibližně o dvě minuty. Dále bylo zjištěno zlepšení tavicího procesu při překročení teploty likvidu průměrnou teplotou roztavené lázně. Práce rovněž popisuje nerovnoměrnost ohřevu obloukem a diskutuje možnosti optimalizace procesu tavení v EOP.

Klíčová slova: *elektrická oblouková pec, stejnosměrný proud, obloukový ohřev, CFD, vrstvení šrotu, tavení*

Hutnické listy – *Metallurgical Journal*
Speciální vydání / Special Issue, roč. / vol. LXXIX
ISSN Online: 3029-8350

1. Introduction

Electric arc furnaces (EAFs) play a critical role in modern steelmaking, contributing a significant fraction of production capacity in North America. In particular, DC EAFs present some key advantages in energy efficiency, power input flexibility, and consistent spatial melting due to the central location of the arc, among others [1]. The melting process in EAFs is influenced by various factors, with electrical power input being a key determinant of melting performance. Understanding and accurately predicting melting behavior under different electrode power conditions is essential for optimizing operational efficiency and minimizing energy consumption.

CFD modelling offers key advantages for analysing and optimizing complex EAF processes. It provides detailed, spatially resolved insights into process behavior which can be difficult to measure directly and enables analysis of parameters like electrode power in isolation, without trial-and-error testing. Once validated, CFD can also be used to optimize operations, improving EAF efficiency and reliability.

Many researchers have utilized simulation methods of various techniques (including CFD) to investigate components of the EAF process. Kazak et al. conducted numerical modelling to investigate the electromagnetic, temperature, and hydrodynamic distributions in a DC EAF. It was found that raising the bottom electrode to the electrode radius above the fettle surface reduced shear stress by 30%, while lowering it by the same distance below the surface reduced stress by 10% [2].

Fathi et al. developed a computational model and algorithm to estimate the arc energy distribution in an EAF, accounting for conductive, convective, and radiative heat transfer. The proposed algorithm uses a channel arc model (CAM) to reduce computational load, requiring only arc length and arc current as inputs. Results show high similarity with experimental data, validating the model effectiveness while maintaining low computational complexity [3].

Samet et al. developed and compared three computational approaches to calculate optimal set-points for series reactors and transformer taps in a DC EAF. Results highlight that improving the transferred power by adjusting transformer taps and reactor configurations can significantly enhance EAF productivity [4]. Martell-Chávez et al. introduced the concept of “useful arc power” and used a thermal model to theoretically estimate the peak arc power in AC-EAFs. The influence of arc length and stability on energy efficiency was analysed. Industrial-scale EAF tests confirmed that optimizing current setpoints can improve energy efficiency [5]. Bhonsle et al. developed a novel time domain EAF model to investigate power quality issues in electric arc furnaces, focusing on non-linear loads that introduce voltage flicker and harmonic distortion in distribution networks.

Simulations conducted in the SIMULINK/MATLAB environment confirmed the model effectiveness in analysing and addressing power quality problems in EAF operation [6]. Logar et al. performed a statistical analysis of over 2500 heats of EAF data, focusing on how input feeds and the carbon-to-oxygen ratio affect electrical energy consumption (EEC). The study found that besides scrap weight and tapping temperature, fluctuations in the added carbon and oxygen also significantly impact EEC. These insights can help identify operational improvements to reduce energy consumption [7].

The subject of this study is to simulate and validate a real-world DC EAF operation based on a furnace operated by SSAB Americas and to use the integrated model for prediction. This study focuses on the impact of electrode power input on melting performance.

Hutnické listy – *Metallurgical Journal*
Speciální vydání / Special Issue, roč. / vol. LXXIX
ISSN Online: 3029-8350

Three cases with different electrode power conditions were developed: the baseline case and two cases with electrical power input reduced to 90% and 80% of the baseline, respectively. The operation time considered in this study starts from the moment the electrode begins operation, covering the bore-in stage and extending 20 minutes beyond this stage.

2. Methodology

The focus of this paper is on the impact of electrode power on melting performance. **Fig. 1** provides a schematic overview of the comprehensive CFD DC scrap melting model developed by researchers at Purdue University Northwest for the Steel Manufacturing Simulation and Visualization Consortium (SMSVC). This comprehensive CFD EAF scrap melting simulator is used to simulate the melting process in a real DC EAF operation provided by SSAB. The simulator consists of three sub-models: the scrap melting model, the coherent jet model, and the electric arc model.

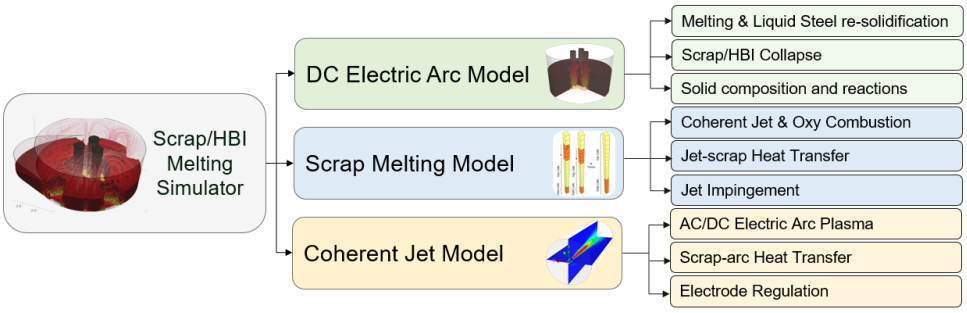

Fig. 1 Schematic overview of the comprehensive CFD DC Scrap Melting Model

Obr. 1 Schematický přehled komplexního CFD modelu DC Scrap Melting Model

Details of these models are presented in previous publications [9], while the functionality is summarized here. The DC electric arc model uses constant impedance control to maintain arc voltage and current, with arc impingement modelled as additional liquid bath momentum. Arc heating distribution is determined using lab-scale 2D simulations and a database of DC parameters [3], integrated into the scrap melting model to capture heating effects in industrial EAF scenarios. Additionally, the coherent jet model [8] accounts for combustion reactions and heat exchange between gas and solid phases, using species conservation equations and heat transfer coefficients. Heat transfer is determined by temperature-dependent expressions.

The scrap melting model uses a two-phase (liquid and gas) Eulerian-Eulerian approach for modelling fluids and incorporates solid-liquid mass transfer, inter-phase forces, and arc-induced momentum. Solid scrap melting and collapse is modelled using a dual-cell approach. Melting and re-solidification are captured via latent heat and effective specific heat capacity, with complete details can be found in previous publications [9] [10]. **Fig. 2** demonstrates the flowchart specific to this study for investigating the effect of electric arc power on melting performance. After preprocessing the operational data provided by SSAB, the arc profile, scrap layering condition, and burner profile needed for the simulation are provided as inputs to the electric arc model, scrap melting model, and coherent jet model, respectively. The outputs of the simulation model, such as melting rate, temperature, and electrode motion, can be used for validation by comparing results with real-world data. Once the model is validated, scenario cases with different electrode power profiles are established to study the impact of electrode power.

Hutnické listy – *Metallurgical Journal*
Speciální vydání / Special Issue, roč. / vol. LXXIX
ISSN Online: 3029-8350

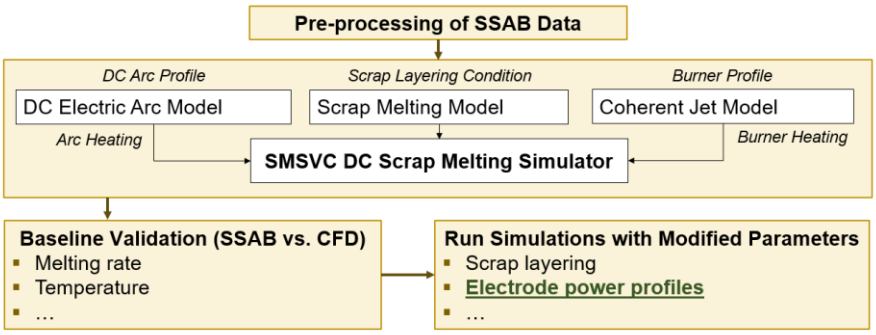

Fig. 2 Flowchart for the Effect of Electrode Power on Melting Performance

Obr. 2 Schéma vlivu výkonu elektrody na vlastnosti tavení

3. Simulation Parameters

Fig. 3 illustrates the timeline of an SSAB tap-to-tap process. The first 40 minutes employ a hold-fire mode for the burners with no electrode power. In this stage, two scrap buckets are charged while the shell awaits the next opportunity for the electrode and melting. The following 37 minutes comprise the melting and refining stage, when both the electrode and burners are on. The entire process lasts 87 minutes.

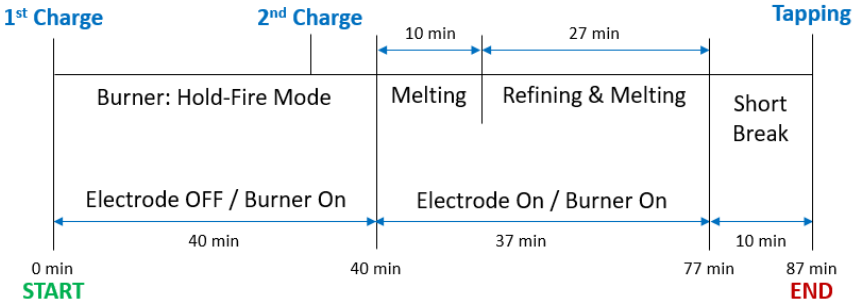

Fig. 3 SSAB DC EAF Tap-to-Tap Process Timeline

Obr. 3 Časová „tap-to-tap“ osa v elektrické obloukové peci SSAB DC

Tab. 1 and **Fig. 4** separately present the scrap layering condition and the burner profile. The scrap density varies across different locations in the furnace. In the simulation, this variation is captured by incorporating the bulk density and weight of each material according to the actual SSAB recipe. There are eight layers of scrap in the first bucket and one layer in the second bucket. Regarding the burner profile, all burners operate in combustion mode before 3000 seconds. After this, the oxygen injection rates for burners 1 and 3 increase significantly, initiating the lancing mode, while burners 4 and 5 continue operating in combustion mode. The figure on the right side of **Fig. 4** shows the locations of these four burners, with burner 2 turned off during this heat.

Tab. 1 Scrap Layering Conditions / **Tab. 1** Podmínky pro vrstvení šrotu

	Commodity	**Weight [kgs]**
1st Bucket	PROCREVERT/2HM/HM1/CAST FE/PIT SCRAP/#1.5 DE BUNDLES/MXTN/FRAG	108,636.4
2nd Bucket	FARG	53,090.9

Hutnické listy – *Metallurgical Journal*
Speciální vydání / Special Issue, roč. / vol. LXXIX
ISSN Online: 3029-8350

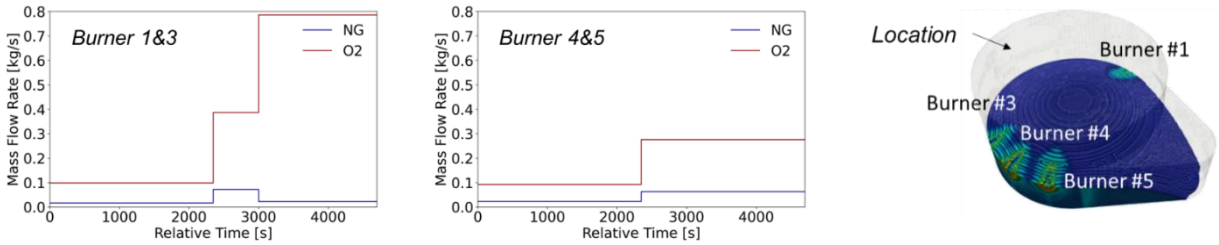

Fig. 4 Burner Profiles / **Obr. 4** Profily hořáků

Fig. 5 shows the different input profiles for the three study cases, which vary in arc power, arc length, and current. In this study, the arc power is adjusted by changing the arc current, which consequently causes changes in both arc length and current. The arc power levels in the three cases are set at 100% (baseline case, based on SSAB actual power profile), 90%, and 80%, respectively.

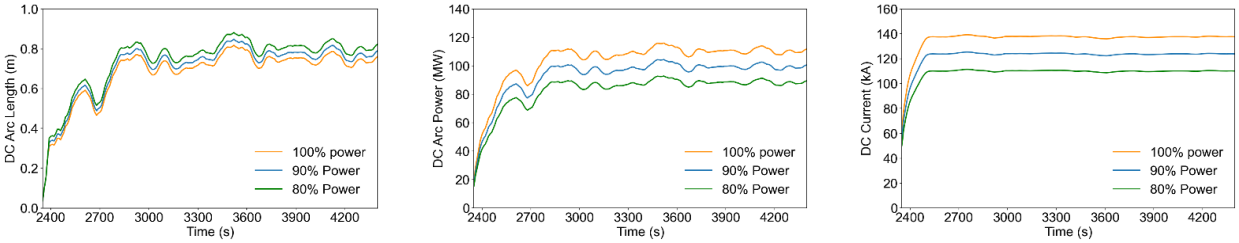

Fig. 5 Different Input Profile for Three Parametric Study Cases (80%, 90% & 100%)

Obr. 5 Různé vstupní profily pro tři parametrické případové studie (80%, 90% a 100%)

Tab. 2 shows the detailed setup for these three cases with different inputs. The only differences among the three cases are the inputs shown in **Fig. 5**. Besides this, all three cases have the same number of burners, burner power input, and initial recipe.

Tab. 2 CFD Cases Setup: Different Power Condition / **Tab. 2** Nastavení CFD modelů: Různé podmínky napájení

Case	Power	Total Electrode Power Input	Burner	Total Burner Input	Recipe
1	100% Power	65412 kwh	4 Burners	~6.42 kwh	2 Buckets 7 Layers
2	90% Power	58871 kwh			
3	80% Power	52329 kwh			

4. Validation

Results shown in this section are up to 4500 seconds, representing approximately 96% of the actual SSAB operation. The method for validation is to compare the melting rate predicted by the CFD simulation with the one expected in actual SSAB operation. Also, the average melting temperature is compared with data collected near tapping.

Fig. 6 shows the solid mass and liquid mass over time from the CFD results, while **Tab. 3** presents the differences between the SSAB data and simulation results. The average melting rate for the first 2170 seconds of melting in this case is 59 kg/s. For SSAB's industrial operation, assuming all scrap is melted at the end of the heat, the average melting rate is 68 kg/s.

Hutnické listy – *Metallurgical Journal*
Speciální vydání / Special Issue, roč. / vol. LXXIX
ISSN Online: 3029-8350

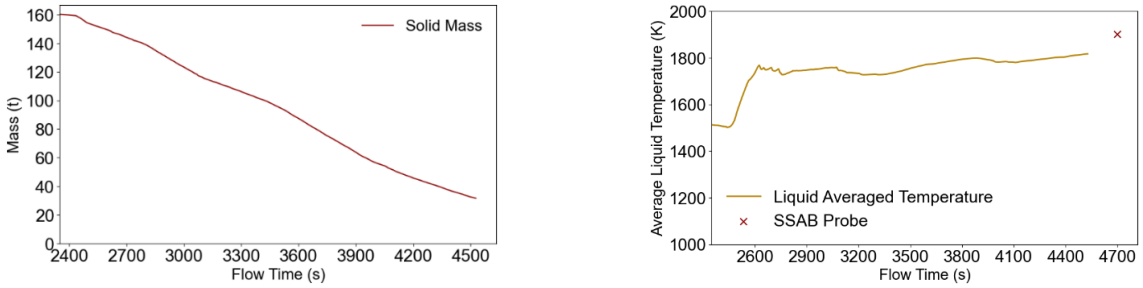

Fig. 6 Simulation Results: Liquid Mass, Solid Mass & Average Liquid Temperature

Obr. 6 Výsledky simulace: podíl kapalné fáze, podíl pevné fáze a průměrná teplota kapalné fáze

Therefore, the difference at this stage is approximately 13.2%. It should be noted that the current case does not include the effect of arc shrouding by foamy slag, which is to be considered in future simulations. This effect is anticipated to reduce energy losses and increase the simulated average melting rate. **Fig. 6** also shows the average liquid temperature over time. The temperature increases rapidly during the first 400 seconds, then stabilizes. In SSAB heat the liquid temperature reached 1902 K near the end of the operation. Therefore, the current difference between average liquid temperature in CFD simulation and the one provided by SSAB probe is 4.5%.

Tab. 3 Difference between SSAB Data and Simulation Results / **Tab. 3** Rozdíl mezi daty SSAB a výsledky simulace

	SSAB	CFD	Difference
Melting Rate (kg/s)	68	59	13.2%
Molten Steel Temperature (k)	1902	1816	4.5%

5. Results

Fig. 7 illustrates the simulation results of the bore-in stage and melting stage. In this study, it is assumed that only vertical collapse occurs during melting. The bore-in stage ends at 2510 seconds and lasts for 160 seconds, with re-solidification observed beneath the electrode tip. Following the bore-in stage is the main melting stage, where the melting pattern goes from the inside to the outside and from bottom to top.

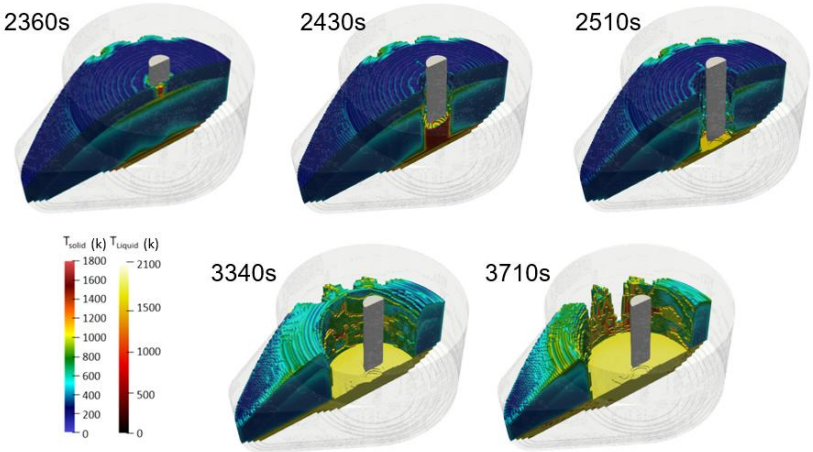

Fig. 7 Simulation Results: Bore-in Stage & Melting Stage

Obr. 7 Výsledky simulace: Počáteční a hlavní fáze tavení

Hutnické listy – *Metallurgical Journal*
Speciální vydání / Special Issue, roč. / vol. LXXIX
ISSN Online: 3029-8350

Fig. 8 shows the simulation results for the three cases with different electrode power inputs. The bore-in rate for the baseline case (100% power) is the fastest (see left **Fig. 8**), as expected. Regarding energy transfer, the total energy transferred from the electrode to the solid scrap and molten steel is plotted (center). The peak of the total energy input for the baseline case can reach 120MW. However, the energy received by the scrap is less than 120MW due to common energy losses during operation. In the plot showing the energy transferred to the solid only (right side), it can be observed that the energy transferred to the solid decreases after the bore-in stage is completed. This is because the electrode tip begins to heat the molten steel bath, causing more energy to be transferred to the liquid phase instead.

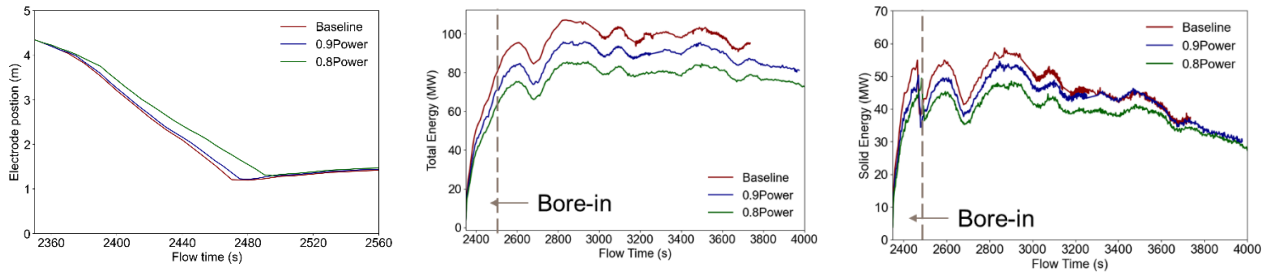

Fig. 8 Simulation Results: Electrode Position & Energy Transfer Distribution

Obr. 8 Výsledky simulace: Poloha elektrod a rozložení přenosu energie

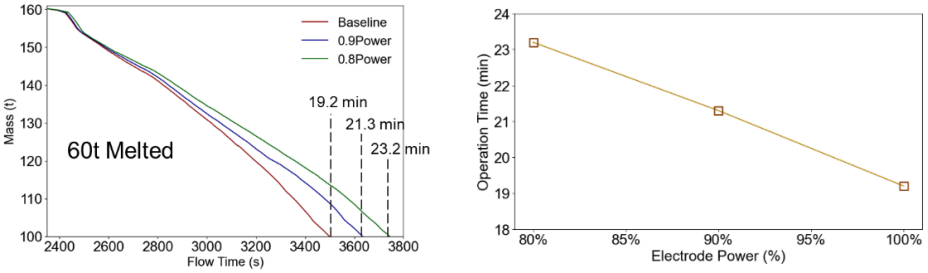

Fig.9 Time Needed to Melt 60 tonnes of Scrap

Obr. 9 Doba potřebná k roztavení 60 tun šrotu

Since different energy inputs lead to varying energy transfer distributions, the melting performance of these three cases with different electrode power inputs will also differ. **Fig. 9** illustrates the change in solid mass after the electrode power is turned on. The red line represents the case with the highest electrode power input, showing the fastest solid melting rate. Comparing the time needed to melt the same amount of solid scrap (60 tonnes), it is observed that it takes 19.2 minutes to melt 60 tonnes of scrap when the electrode power input is 100%. When the power is decreased to 90%, the melting time is increased to 21.3 minutes, a difference of 2.1 minutes, as shown in **Tab. 4**. The plot on the right in **Fig. 9** shows the near-linear relationship between operation time and electrode power.

Tab. 4 Time and Electrode Power Input Needed to Melt 60 tonnes of Scrap
Tab. 4 Čas a příkon elektrod potřebný k roztavení 60 tun šrotu

Case	Time Needed to Melt 60 t	Difference	Electrode Energy Input
100% Power	19.2 min		31,486 kWh
90% Power	21.3 min	2.1 min	31,341 kWh
80% Power	23.2 min	4.0 min	31,010 kWh

Hutnické listy – *Metallurgical Journal*
Speciální vydání / Special Issue, roč. / vol. LXXIX
ISSN Online: 3029-8350

Tab. 4 focuses on the melting time, while **Tab. 5** presents the average melting rate for the first 20 minutes of melting. This set of data does not show a linear trend. When the electrode power is reduced from 100 % to 90%, the average melting rate decreases by approximately 14%. However, the difference drops to 23% when the power is decreased from 100% to 80%.

Tab. 5 Average Melting Rate for the First 20 Minutes / **Tab. 5** Průměrná rychlost tavení během prvních 20 minut

Case	Melting Rate for First 20 Minutes	Difference (%)
100% Power	53.9 kg/s	
90% Power	46.4 kg/s	14 %
80% Power	41.3 kg/s	23 %

To explain the non-linear relationship observed here between electrode power input and the average melting rate for the first 20 minutes, **Fig. 10** presents the instantaneous melting rate for the three cases. Overall, during the bore-in stage, the melting rate increases and then remains relatively constant, with minimal differences between the three cases at this point. Subsequently, each case exhibits a distinct increase at different times.

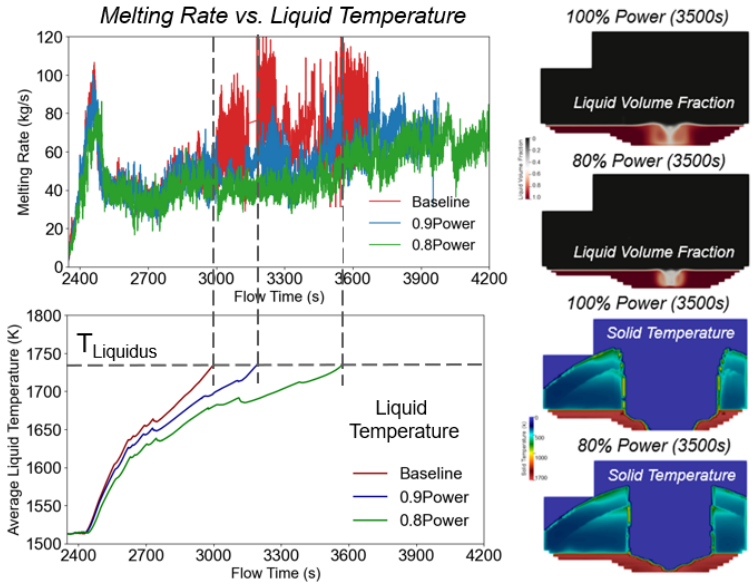

Fig. 10 The Impact of Liquid Temperature on Melting Performance

Obr. 10 Vliv teploty kapalné fáze na vlastnosti tavení

The red line, representing the highest power input, consistently shows the fastest melting rate. However, a noticeable increase in the melting rate only occurs after approximately 3000 seconds. In comparison, for the 80% power case (green line), this increase begins around 3600 seconds. The plot below also indicate that the average molten steel temperature influences the melting rate. The dashed line represents the liquidus temperature, approximately 1734 K. It can be seen from these two plots that once the average molten steel temperature of the entire bath exceeds the liquidus point, the melting rate begins to increase significantly, driven by convection from the liquid steel to the melting solid material in addition to the radiation heat transfer provided directly from the arc. This convection can transport heat to a broader portion of the solid scrap at the bottom of the furnace compared to radiation alone. This trend is observed consistently across all three cases.

Hutnické listy – *Metallurgical Journal*
Speciální vydání / Special Issue, roč. / vol. LXXIX
ISSN Online: 3029-8350

With a higher electrode energy input, the liquid temperature rises more quickly, enabling the liquid phase to begin contributing to the melting process earlier in the 100% power case. This leads to a faster overall melting rate within the first 20 minutes. This is further confirmed by the two contours that show the liquid volume at the same moment. In the 100% power case, more molten steel is present, increasing the contact area of liquid steel with solid scrap and allowing the liquid phase to support the melting process more effectively.

Additionally, the liquid temperature plot demonstrates that the 80% power case requires a longer time to reach the liquidus temperature. This delay can be attributed to non-uniform heating, which makes it more challenging to heat distant regions when the energy input is lower.

The two contours also illustrate the liquid volume at the same time point, highlighting the much stronger heating effect in the baseline case, which helps to extend the temperature rise further into the distant region. Finally, the two contours below show the corresponding solid temperature distribution. From the melting pattern, the molten steel in this case is already assisting the melting process, as indicated by the clear vertical collapse.

6. Conclusions

This study focused on the simulation and validation of a SSAB DC-EAF heat. A discrepancy of approximately 13.2% in the melting rate and 4.5% in the liquid temperature was observed between CFD and actual data. The accuracy of the CFD simulation during the refining stage can be improved through the consideration of slag effects.

Furthermore, electrode power input was identified as a major determinant of melting performance. Variations in DC power input result in different arc current and arc length values, directly influencing the melting rate. It was found that each 10% reduction in arc energy increased the melting time by approximately two minutes.

Additionally, a peak in the melting rate was observed during the bore-in stage, and a significant boost in the melting rate was triggered once the average molten bath temperature exceeds the liquidus point.

References

[1] ODENTHAL, H.-J., KEMKMINGER, A., KRAUSE, F., SANKOWSKI, L., UEBBER, N. and VOGL, N., 2018. Review on modelling and simulation of the electric arc furnace (EAF). *Steel Research International*, 89(1).

[2] KAZAK, O., 2013. Modelling of vortex flows in direct current (DC) electric arc furnace with different bottom electrode positions. *Metallurgical and Materials Transactions B*, 44, pp.1243-1250.

[3] FATHI, A., SABOOHI, Y., ŠKRJANC, I. and LOGAR, V., 2015. Low computational-complexity model of EAF arc-heat distribution. ISIJ International, 55(7), pp.1353–1360.

[4] SAMET, H., GHANBARI, T. and GHAISARI, J., 2014. Maximizing the transferred power to electric arc furnace for having maximum production. *Energy*, 72, pp.752–759.

[5] MARTELL-CHÁVEZ, F., RAMÍREZ-ARGÁEZ, M., LLAMAS-TERRES, A. and MICHELOUD-VERNACKT, O., 2013. Theoretical estimation of peak arc power to increase energy efficiency in electric arc furnaces. *ISIJ International*, 53(5), pp.743–750.

[6] BHONSLE, D.C. and KELKAR, R.B., 2016. Analyzing power quality issues in electric arc furnace by modelling. *Energy*, 115, pp.830–839.

[7] LOGAR, V. and ŠKRJANC, I., 2021. The influence of electric-arc-furnace input feeds on its electrical energy consumption. Journal of Sustainable Metallurgy, 7, pp.1013–1026.

[8] CHEN, Y., LUO, Q., RYAN, S., BUSA, N., SILAEN, A.K. and ZHOU, C.Q., 2022. Effect of coherent jet burner on scrap melting in electric arc furnace. *Applied Thermal Engineering*, 212, 118596.

[9] WANG, S., UGARTE, O., RYAN, S., OKOSUN, T. and ZHOU, C.Q., 2024. Computational fluid dynamics simulation of industrial electric arc furnace operation: validation and performance of melting phenomena. *Steel Research International*, p.2400509.

[10] CHEN, Y., RYAN, S., SILAEN, A.K. and ZHOU, C.Q., 2022. Numerical investigation of AC electric arc plasma heat dissipation in EAF. *Ironmaking & Steelmaking*, 49(3), pp.255–267.